Supplementary Information

Electrochemically robust oxide-supported dendritic Pt and Ir nanoparticles for highly effective polymer electrolyte membrane-unitized regenerative fuel cells

Young-Jin Ko [a†], Hyunchul Kim [a,b†], Woong hee Lee [a], Man Ho Han [a], Cheoulwoo Oh [a], Chang Hyuck Choi [c], Woong Kim [b], Jeong Min Baik [d,e], Jae-Young Choi [d,e], Peter Strasser [f*] and Hyung-Suk Oh [a,d,e*]

[a] Clean Energy Research Center, Korea Institute of Science and Technology, Hwarang-ro 14-gil 5, Seongbuk-gu, Seoul 02792, Republic of Korea

[b] Department of Materials Science and Engineering, Korea University, 145 Anam-ro, Seongbuk-gu, Seoul 02841, Republic of Korea

[c] Department of Chemistry, Pohang University of Science and Technology (POSTECH), Pohang 37673, Republic of Korea

[d] School of Advanced Materials Science & Engineering, Sungkyunkwan University (SKKU), Suwon, 16419, Republic of Korea

[e] KIST-SKKU Carbon-Neutral Research Center, Sungkyunkwan University (SKKU), Suwon 16419, Republic of Korea

[f] Department of Chemistry, Chemical Engineering Division, Technical University Berlin, Berlin 10623, Germany

[†] These authors contributed equally to this work.
*Corresponding Authors
E-mail: pstrasser@tu-berlin.de (P. Strasser), hyung-suk.oh@kist.re.kr (H.-S. Oh)
Tel.: +82 (0)2 958 5292
Fax: +82 (0)2 958 5890

Table of Contents

Statement S1. The overall synthesis mechanism of ATO and ND nanoparticles.

The overall process for synthesis of mesoporous ATO involved the following steps:

I. Formation of Sn-tetradecylamine complex: $SnCl_4$ reacts with ethanol to form $Sn(OC_2H_5)_4$ complex, as indicated by the following reaction.

$$SnCl_4 + 4C_2H_5OH \rightarrow Sn(OC_2H_5)_4 + 4HCl$$

$Sn(OC_2H_5)_4$ is slowly hydrolyzed and then assembled with TDA surfactant in acidic ethanol solution.

II. Hydrolysis and condensation step: The white precipitates are observed when NH_4OH is added to increase the pH. As the antimony doping amount increases, the color of precipitate is observed to light-yellow.

III. Formation of tetradecylamine-SnO_2 phase: Micelles of the tetradecylamine shells on metal oxides are in an intermediate. A related structure was obtained via an alkylamine-$Sn(OC_2H_5)_4$. Tetradecylamine further induces non-covalent bonding between metal oxide and NH_2 functional group by hydrogen bonding.

IV. Hydrothermal treatment for crystallization: Hydrothermal treatment improved thermal and chemical stability by increasing the crystallinity of the oxide.

The overall process for synthesis of PtND and IrND involved the following steps:

I. PtND was formed by seed-mediated growth mechanism. Initially formed nuclei act as seeds for the additional deposition of precursors during the wet chemical reduction reaction.[1, 2] PtND was synthesized through autocatalytic growth of metallic Pt phases from initially formed Pt seeds in the presence of cationic surfactant (TTAB) and slow reducing agent (AA).

II. IrND was formed by aggregation-based growth mechanism. Under conditions where a large number of Ir nanoparticles form rapidly, the smaller nanoparticles aggregate to minimize the total surface energy. Cationic surfactant (TTAB) with intermediate binding affinities for metal ions provide adequate protection from severe aggregation between Ir nanoparticles. However, weak dispersion and inefficient stabilization of Ir nanoparticles lead to self-aggregation of Ir nanoparticles, resulting in IrND formation.[3-5]

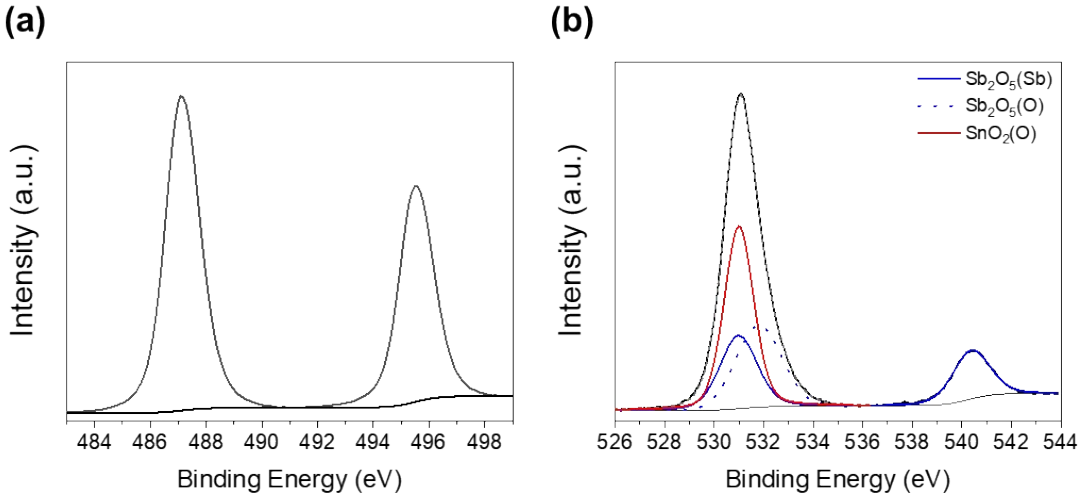

Fig. S1. (a) Sn and (b) Sb 3d XPS spectra of ATO supporter. Since the Sb $3d^{3/5}$ peak and the O 1s peak overlapped, the peak was deconvoluted. The doping ratio of Sb was calculated as 10 at%.

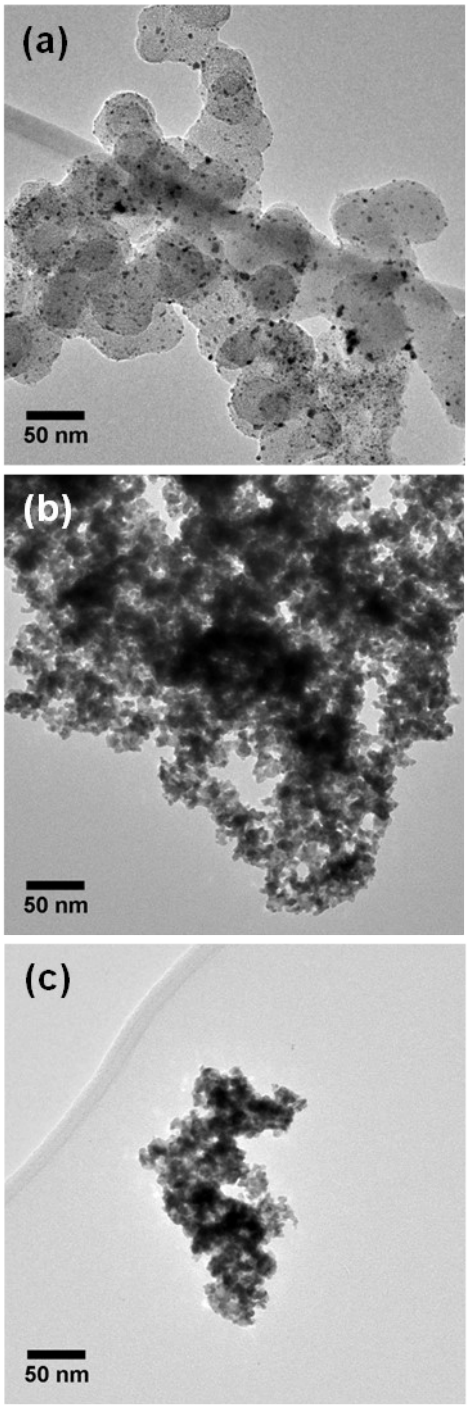

Fig. S2. Low-magnitude TEM image of (a) Pt-Ir/C, (b) Pt black, and (c) Ir black catalysts

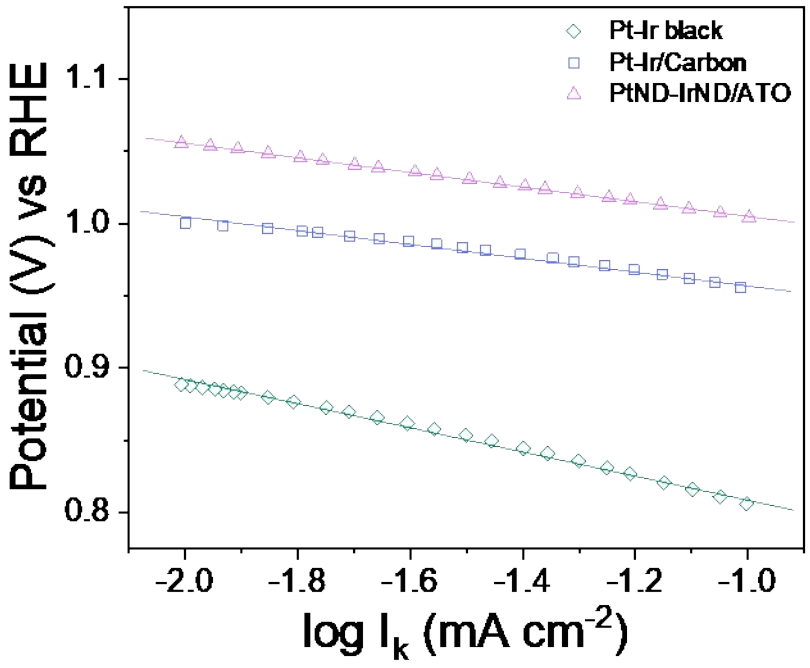

Fig. S3. Tafel plots of electrocatalysts for the ORR in 0.05 M H_2SO_4 solution. The rotating speed was 1600 rpm.

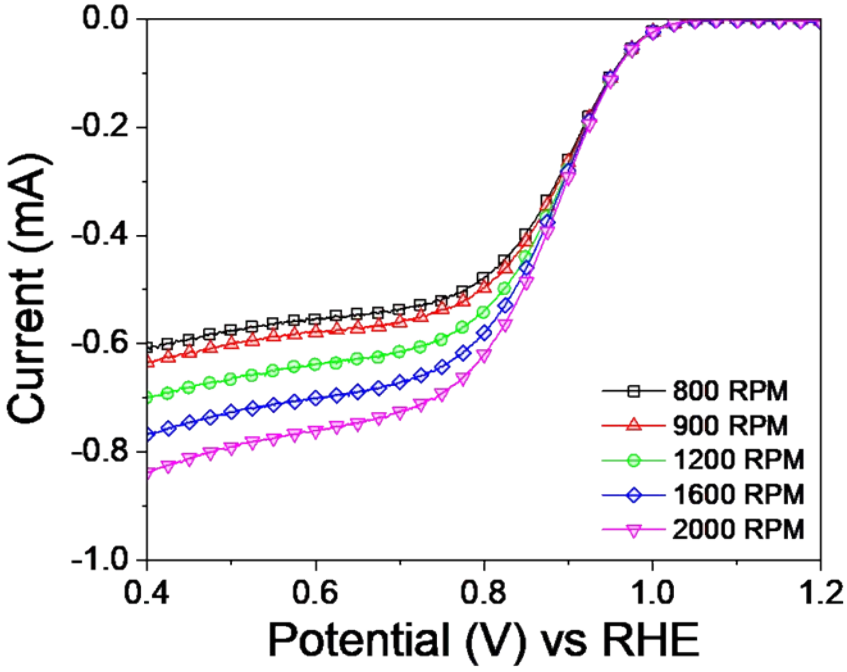

Fig. S4. Polarization curves for PtND-IrND/ATO catalyst at various rotation speeds in O_2-saturated 0.05M H_2SO_4 solution.

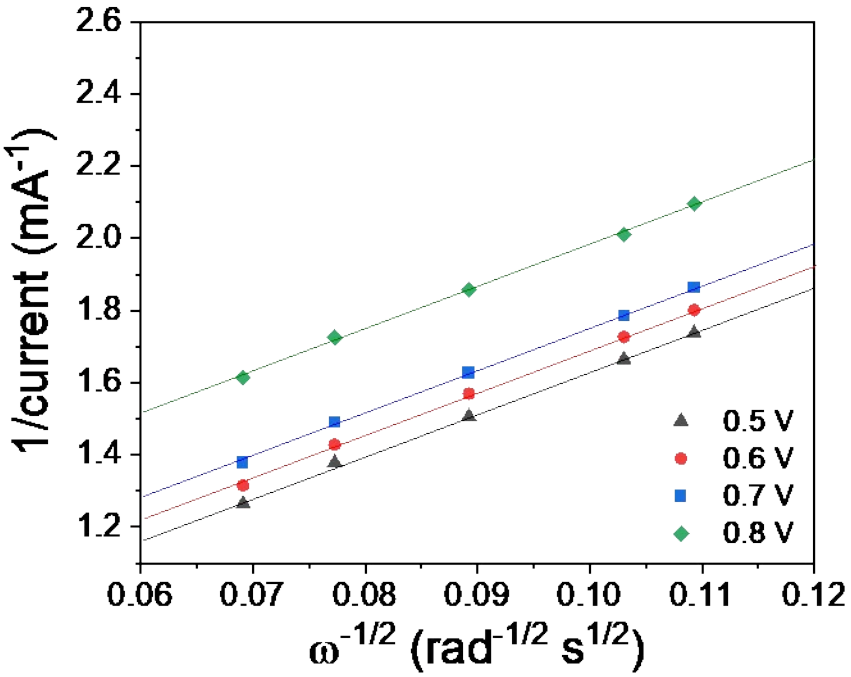

Fig. S5. Koutecky-Levich plot of PtND-IrND/ATO catalyst for the determination of the number of electrons transferred during the ORR. The *B* factor was calculated from the slope of the Koutechy-Levich plot using the equation in the references.[6]

Table S1. Round trip (RT) efficiencies of electrocatalysts for URFC operation at 0.5 A cm^{-2}.

Catalyst	Current density (A cm^{-2})	V_{FC} (V)	V_{WE} (V)	V_{RT} (%)
Pt-Ir Black	0.5	0.654	1.617	40.4
	1.0	0.469	1.870	25.1
Pt-Ir/Carbon	0.5	0.704	1.520	46.3
	1.0	0.598	1.697	35.2
PtND-IrND/C	0.5	0.727	1.636	44.4
	1.0	0.626	1.796	34.9
Pt-Ir/ATO	0.5	-	-	-
	1.0	-	-	-
PtND-IrND/ATO	0.5	0.747	1.491	50.1
	1.0	0.642	1.625	39.5

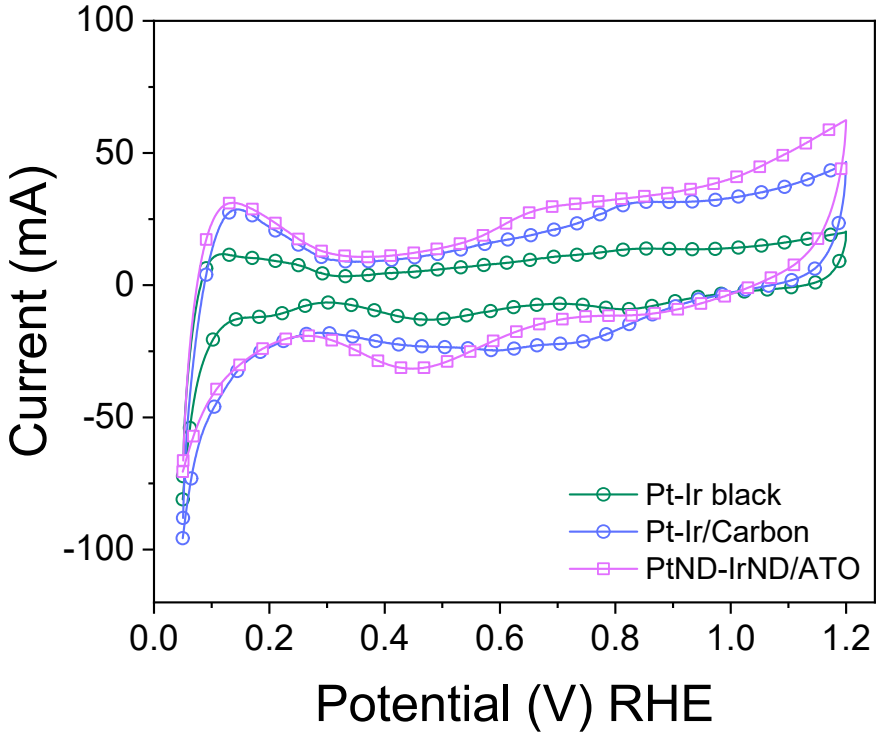

Fig. S6. Cyclic voltammograms of MEAs for electrocatalysts at scan rate of 50 mV s^{-1}. The cathode was purged with N_2 gas to remove all O_2 gas.

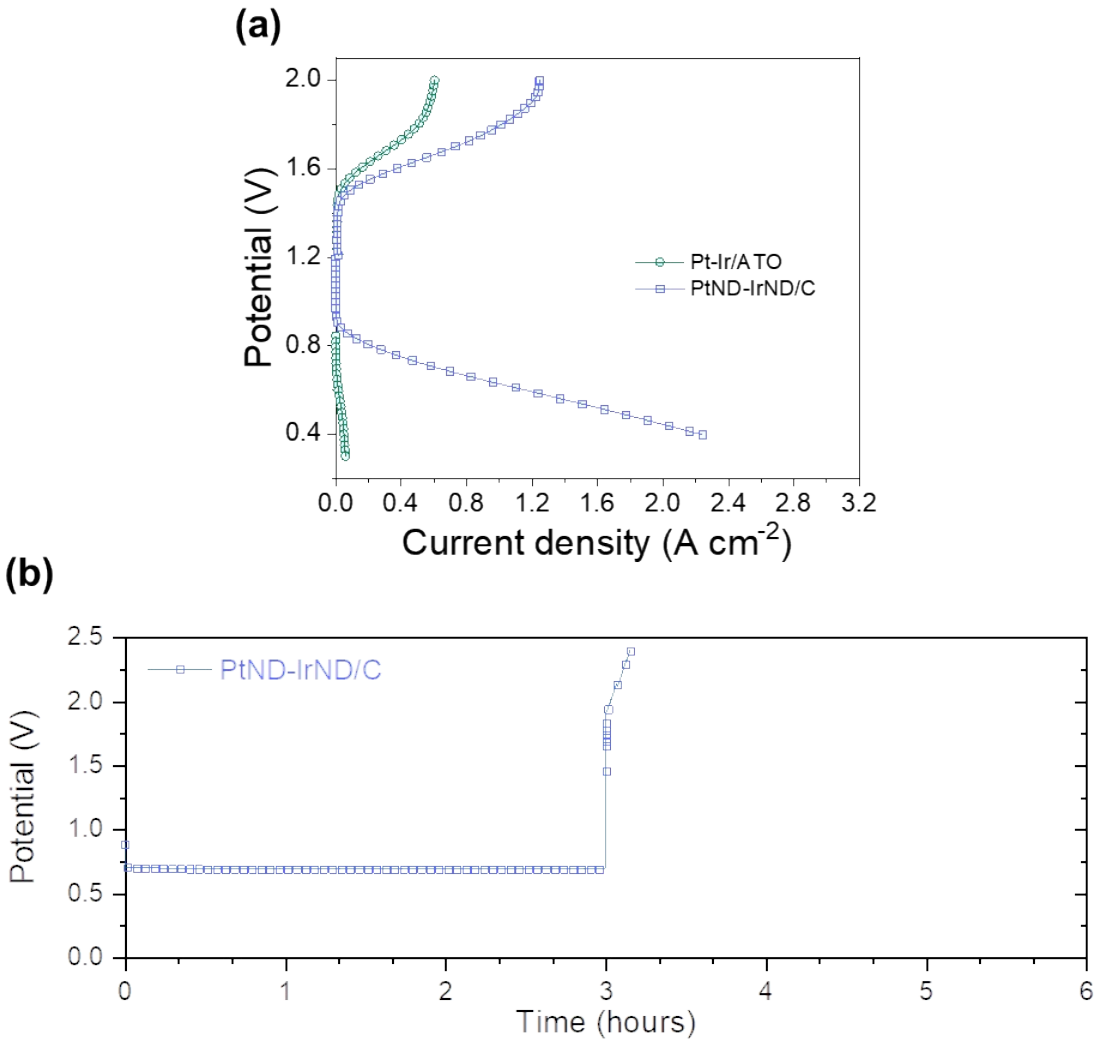

Fig. S7. (a) URFC performance of Pt-Ir/ATO, and PtND-IrND/C catalysts. (b) Long-term URFC operation at 0.5 A cm^{-2}.

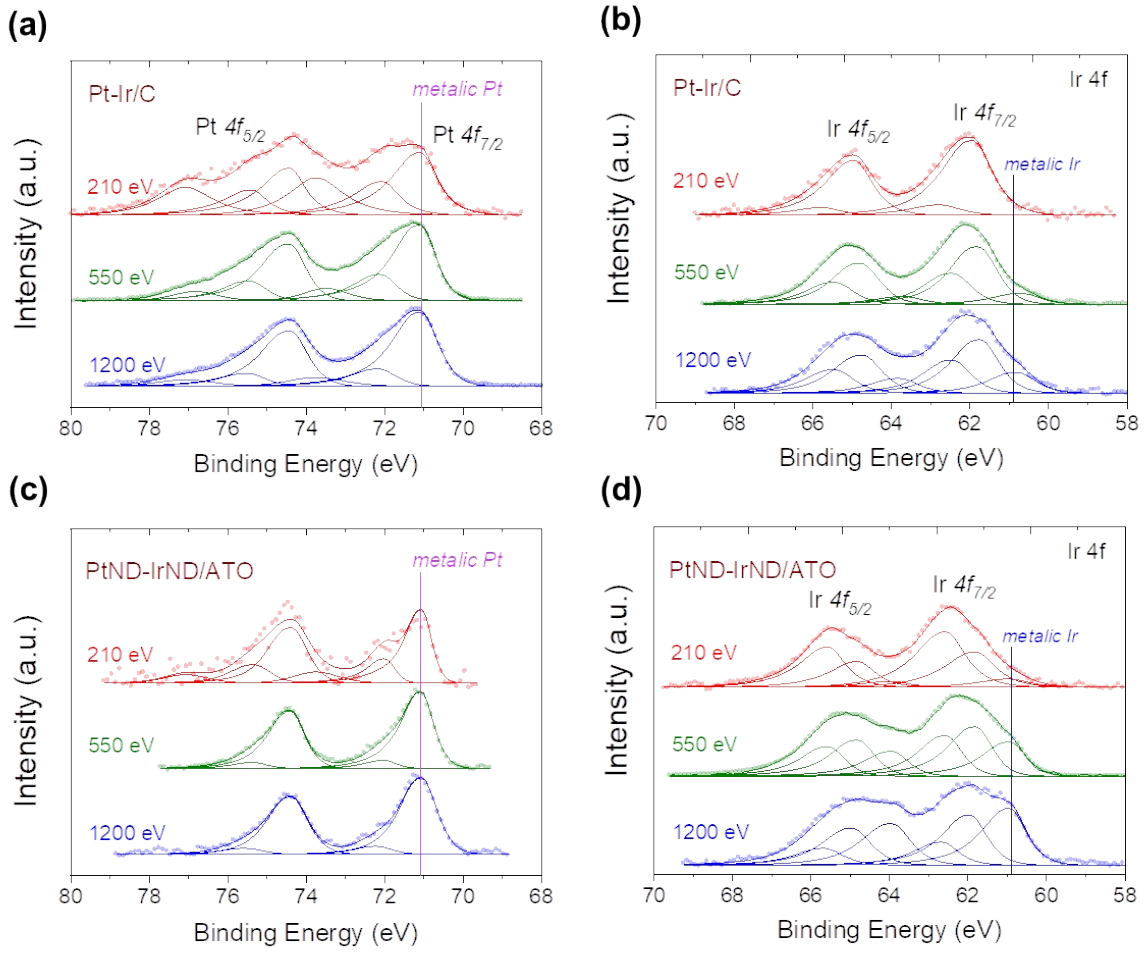

Fig. S8. Depth-resolved Pt and Ir 4f XPS spectra of (a, b) Pt-Ir/C and (c, d) PtND-IrND/ATO catalysts after OER. The photoelectron kinetic energy was 210, 550, and 1200 eV from top to bottom. Magenta line and blue line indicated metallic Pt and Ir, respectively.

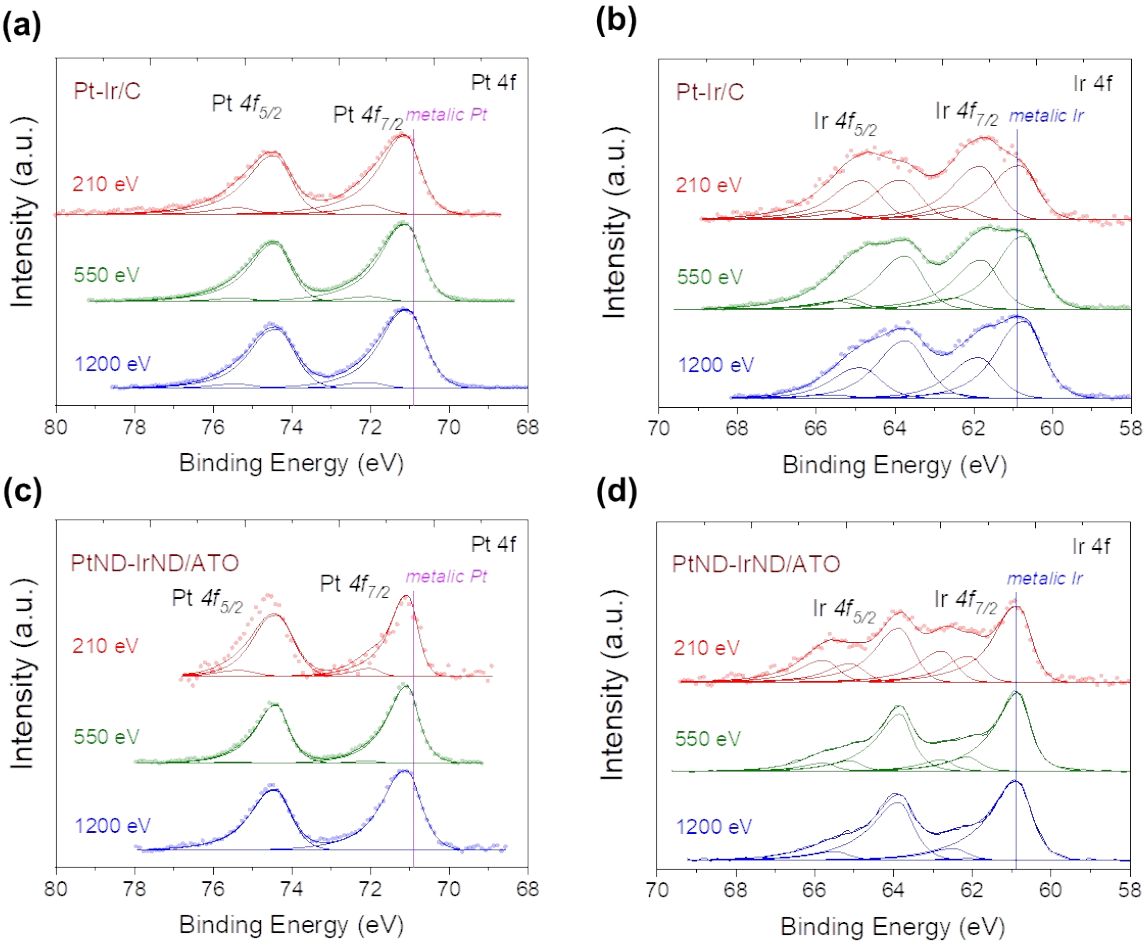

Fig. S9. Depth-resolved Pt and Ir 4f XPS spectra of (a, b) Pt-Ir/C and (c, d) PtND-IrND/ATO catalysts after ORR. The photoelectron kinetic energy was 210, 550, and 1200 eV from top to bottom. Magenta line and blue line indicated metallic Pt and Ir, respectively.

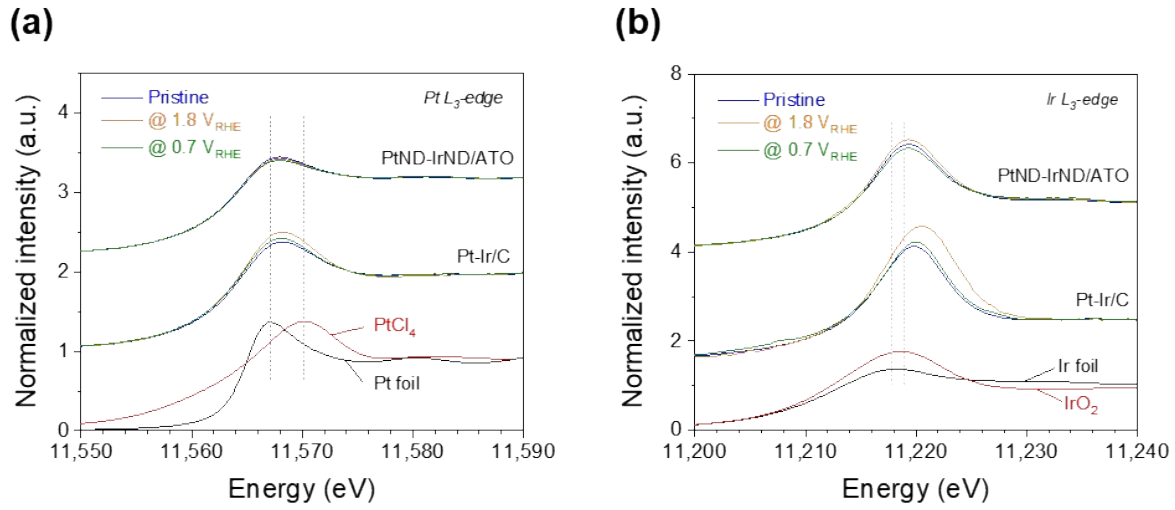

Fig. S10. *In-situ/Operando* (a) Pt and (b) Ir L_{III}-edge XANES spectra of Pt-Ir/C, PtND-IrND/ATO catalysts. Pt foil, Pt(IV) chloride, Ir foil, and Ir(IV) oxide were used as reference materials.

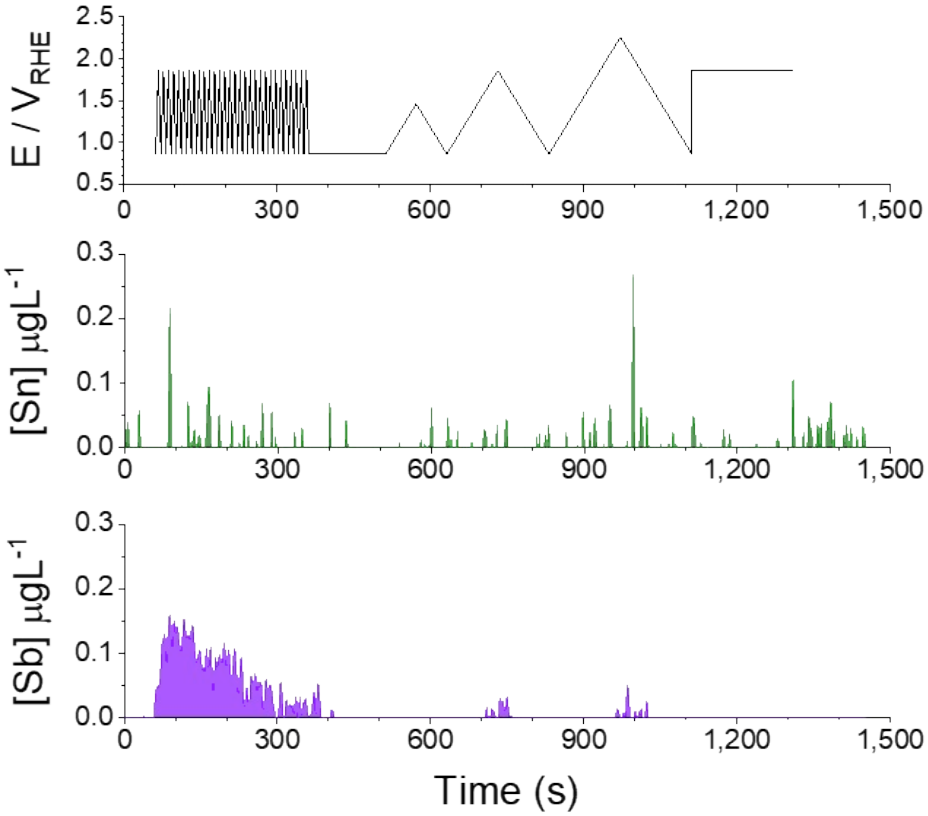

Fig. S11. Real-time Sn and Sb dissolution profiles of PtND-IrND/ATO catalyst under a representative experimental sequence.

Supporting Information References

1. Y. Xia, Y. Xiong, B. Lim and S. E. Skrabalak, *Angew. Chem. Int. Ed.*, 2009, **48**, 60-103.
2. J. Chen, B. Lim, E. P. Lee and Y. Xia, *Nano Today*, 2009, **4**, 81-95.
3. C. Wang, G. Xiao, Y. Sui, X. Yang, G. Liu, M. Jia, W. Han, B. Liu and B. Zou, *Nanoscale*, 2014, **6**, 15059-15065.
4. H. Zheng, R. K. Smith, Y.-w. Jun, C. Kisielowski, U. Dahmen and A. P. Alivisatos, *Science*, 2009, **324**, 1309-1312.
5. N. Ortiz and S. E. Skrabalak, *Angew. Chem. Int. Ed.*, 2012, **51**, 11757-11761.
6. T.-P. Fellinger, F. Hasché, P. Strasser and M. Antonietti, *Journal of the American Chemical Society*, 2012, **134**, 4072-4075.